Nanoscale

PAPER

View Article Online
View Journal | View Issue

Cite this: *Nanoscale*, 2016, **8**, 6173

Ultrathin Cu_2O as an efficient inorganic hole transporting material for perovskite solar cells†

Weili Yu,[a,b] Feng Li,[a] Hong Wang,[a] Erkki Alarousu,[c] Yin Chen,[c,d] Bin Lin,[a] Lingfei Wang,[a] Mohamed Nejib Hedhili,[e] Yangyang Li,[a] Kewei Wu,[a] Xianbin Wang,[f] Omar F. Mohammed[c] and Tom Wu*[a]

Received 5th November 2015,
Accepted 15th February 2016

DOI: 10.1039/c5nr07758c

www.rsc.org/nanoscale

We demonstrate that ultrathin P-type Cu_2O thin films fabricated by a facile thermal oxidation method can serve as a promising hole-transporting material in perovskite solar cells. Following a two-step method, inorganic–organic hybrid perovskite solar cells were fabricated and a power conversion efficiency of 11.0% was achieved. We found that the thickness and properties of Cu_2O layers must be precisely tuned in order to achieve the optimal solar cell performance. The good performance of such perovskite solar cells can be attributed to the unique properties of ultrathin Cu_2O, including high hole mobility, good energy level alignment with $CH_3NH_3PbI_3$, and longer lifetime of photo-excited carriers. Combining the merits of low cost, facile synthesis, and high device performance, ultrathin Cu_2O films fabricated *via* thermal oxidation hold promise for facilitating the developments of industrial-scale perovskite solar cells.

Introduction

The tremendous demands of clean, renewable and environment-friendly energy have stimulated the rapid developments of photovoltaic technologies, and particularly lead halide based perovskite solar cells have attracted lots of recent interest.[1,2] Thanks to the compelling merits of perovskites such as low-cost processing, strong solar absorption, and long carrier diffusion lengths, the power conversion efficiency (PCE) of perovskite solar cells has increased by several folds in a few years to about 20%.[3–10] In both planar and meso-porous structured perovskite solar cells, charge transporting materials play critical roles in the extraction and collection of photo-excited carriers. TiO_2 is routinely used as the electron transporting material (ETM) because of its suitable energy level for electron injection, high electron mobility, good stability and environmental friendliness.[11–13] It is more challenging to select appropriate hole transporting materials (HTMs) which are needed for extracting holes effectively from the perovskite layer while preventing electrons from recombination.[14–22]

To date, reported efficient HTMs include both organic and inorganic semiconductors.[14–23] Organic HTMs, such as 2,2′,7,7′-tetrakis(*N*,*N*-di-*p*-methoxyphenylamine)-9,9′-spirobifluorene (spiro-OMeTAD), poly(3,4-ethylenedioxythiophene): polystyrene sulfonate (PEDOT:PSS), poly-3-hexylthiophene (P3HT) and poly-triarylamine (PTAA), suffer from high cost and low stability. Inorganic HTMs, particularly transition-metal oxides (such as WO_3, MoO_3, and V_2O_5), have merits such as low cost, chemical and thermal stability, as well as high work function.[23] However, to date the progress on developing inorganic HTMs for perovskite solar cells has been limited.[17,18,24] One main reason is that the thickness of transition-metal-oxide HTMs must be controlled within a few nanometers in order to avoid high series resistance,[23] but such ultrathin layers cannot provide complete coverage on perovskite layers with rough surfaces.[24–26] To solve this problem, a feasible strategy is to use the reversed solar cell structure, *i.e.*, metal oxide HTMs are deposited on an ITO substrate first, and then followed by the spin coating of the perovskite layers.[27–30] However, the limited choices of inorganic HTMs reported so far (Table S1†) circumvent the developments of perovskite solar cells with structural variability and processing optimization. More environmentally friendly and efficient inorganic metal oxide semiconductors are in urgent need for serving as HTMs in perovskite solar cells.

[a]*King Abdullah University of Science and Technology (KAUST), Material Science and Engineering, Thuwal 23955-6900, Saudi Arabia. E-mail: Tao.Wu@kaust.edu.sa*
[b]*School of Materials Science and Engineering, Changchun University of Science and Technology, Changchun 130022, P. R. China*
[c]*King Abdullah University of Science and Technology (KAUST), Solar and Photovoltaics Engineering Research Center, Thuwal 23955-6900, Saudi Arabia*
[d]*College of Chemistry and Chemical Engineering, Central South University, Changsha 410083, P. R. China*
[e]*King Abdullah University of Science and Technology (KAUST), Imaging and Characterization Core Lab, Thuwal 23955-6900, Saudi Arabia*
[f]*King Abdullah University of Science and Technology (KAUST), Nanofabrication Core Lab, Thuwal 23955-6900, Saudi Arabia*

†Electronic supplementary information (ESI) available: Experimental details, AFM images, XRD, hysteresis, XPS, EDAX, device stability and statistics. See DOI: 10.1039/c5nr07758c

Cu_2O is a typical p-type semiconductor, which has been studied for decades due to its unique physical properties and applications in areas ranging from photoelectrochemistry[31] to magnetoelectrics[32] and superconductors.[33] A recent theoretical study proposed that Cu_2O might outperform other transition-metal oxides including NiO as HTMs in perovskite solar cells.[34] The unique merits of Cu_2O, such as low cost (Table S2†) and environmental friendliness, make it a promising candidate for solar cell applications. Very recently, in a pioneering work, Zuo *et al.* fabricated Cu_2O and CuO films using *in situ* conversion of CuI films in NaOH aqueous solution.[35] However, the effect of Cu_2O layer thickness on the perovskite solar cell performance as well as the carrier dynamics have not been thoroughly investigated.

Here, we demonstrate that thermally oxidized ultrathin Cu_2O films can serve as an efficient HTM in perovskite solar cells. Ultrathin Cu_2O films were prepared *via* a facile process of Cu sputtering and controlled thermal oxidation, which is simple, suitable for large-scale processing and easy to control the layer thickness. Importantly, this synthesis route is suitable to optimize Cu_2O as the hole-transporting layer in perovskite solar cells. The optical and electrical properties of such ultrathin Cu_2O films were systematically characterized. The results of photoluminescence quenching and exciton relaxation dynamics of the perovskite/Cu_2O bilayers indicate efficient carrier transfer at the perovskite/Cu_2O interface. After optimizing the Cu_2O film thickness to 5 nm, which is probably the thinnest HTM reported to date, perovskite solar cells with a PCE of 11.0% were achieved under AM1.5G solar illumination. Our findings strongly support Cu_2O as a promising inorganic HTM for industrial-scale perovskite solar cell applications.

Results and discussion

The work function of Cu_2O is around 5 eV,[36] which is lower than the valence band edge of $CH_3NH_3PbI_3$ (5.4 eV)[6] and favors hole transfer at the interface (see Fig. 1a). The XRD spectra of the Cu layer (as prepared) and Cu_2O layer (after thermal oxidation at 250 °C in air for 1 hour) are presented in Fig. 1b. The Cu film shows a peak at 43.9°, corresponding to the (111) plane of a face-centered cubic structure. The Cu_2O film shows a peak at 36.9°, which can be assigned to the (111) diffraction of a cubic-structured Cu_2O phase.[37] The ITO glass with 5 nm Cu_2O exhibits a slight brown color. The AFM image of the Cu_2O film is presented in Fig. S1.† The root-mean square roughness (R_{rms}) of the Cu_2O-covered ITO film is 1.79 nm, which is slightly smoother than that of the ITO surface (R_{rms} = 1.96 nm). XPS characterization also confirmed that most of the Cu ions in the films were in the 1+ valence state (Fig. S2†). These results indicate that the ultrathin Cu_2O films can be reliably achieved using the simple oxidation method.

The Cu_2O layers must be as thin as possible because thick Cu_2O layers will suffer from poor transmittance and high resistance. Fig. 1c shows the transmittance spectra of ITO with and without Cu_2O. For bare ITO glass, the transmittance is above 75% when the wavelength is higher than 370 nm. After covering with 5 nm Cu_2O, the transmittance of ITO glass decreases slightly, but it remains above 75% at a wavelength above 420 nm. The absorption coefficient α of the Cu_2O layer is shown in Fig. 1d, which was calculated according to the following formula:

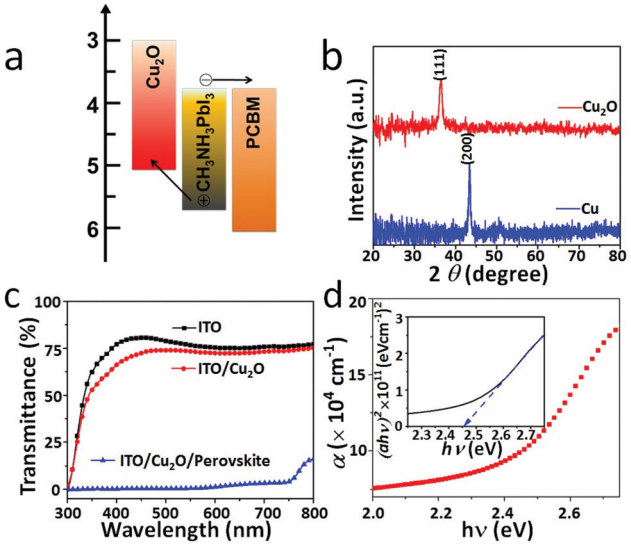

Fig. 1 (a) Energy alignment of the perovskite solar cells with Cu_2O as an HTM and PCBM as an ETM. (b) XRD spectra of Cu and Cu_2O thin films. (c) Transmittance spectra of ITO glass, ITO-Cu_2O and ITO-Cu_2O-perovskite samples. (d) Absorption coefficient of the Cu_2O film and inset is the Tauc plot of the absorption data.

$$\alpha = -\ln T/d \quad (1)$$

where T is the transmittance and d is the film thickness. Fig. 1d indicates that the Cu_2O layer has a high absorption coefficient (>10^5) in the visible range, especially for light with a wavelength below 500 nm. Thus, the Cu_2O layer should be as thin as possible to decrease the absorption. The dependence of transmittance on the Cu_2O thickness is shown in Fig. S3.† From the Tauc plots shown in the inset of Fig. 1d, the bandgap (E_g) of the Cu_2O layer is deduced from:

$$\alpha^n = B(h\nu - E_g) \quad (2)$$

where $h\nu$ is the energy of incident photons and B is a constant. A good fitting was achieved with n = 2, indicating the direct bandgap nature of the Cu_2O film.[37] According to eqn (2), we calculated E_g of the Cu_2O layer as 2.24 eV, which is slightly higher than the value reported in the literature for bulk Cu_2O,[36] which may be related to the quantum confinement in such ultrathin Cu_2O films.

The solar cell structure is presented in Fig. 2a. Ultrathin Cu_2O layers between the ITO glass and perovskite served as the HTM, and $PC_{61}BM$ was introduced as the ETM and hole blocking layer. Compared to the mesoporous perovskite solar cells, the planar ones are easier to fabricate and to scale up.[8,9] The

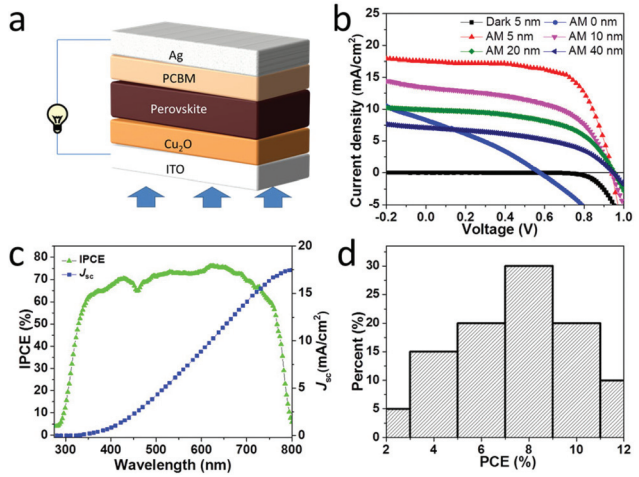

Fig. 2 (a) Structure of the perovskite solar cells. (b) *I*–*V* performances of solar cells with different Cu_2O layer thicknesses in the dark and under illumination (AM 1.5). (c) IPCE spectra of the device with a Cu_2O layer of 5 nm. (d) The statistical histogram plot of PCE for solar cells with 5 nm Cu_2O HTM.

perovskite layers with a thickness of 400 nm were prepared using the two-step method. A 60 °C pre-heated PbI_2 solution (1 M, *N*,*N*-dimethylformamide) was first spin-coated on ITO/Cu_2O. After several minutes of drying, the yellow colored films were dipped into CH_3NH_3I solution (10 mg l^{-1}, isopropanol) for 30 s to convert PbI_2 into $CH_3NH_3PbI_3$, which was accompanied by the change of color from yellow to dark brown. The formation of the perovskite phase was further confirmed by the XRD spectra (Fig. S4†). We also tried the one-step method by spin-coating the mixed solution of $PbCl_2$ and CH_3NH_3I onto ITO/Cu_2O, but no pure perovskite phase was achieved after annealing at 100 °C, which might be related to the surface properties of Cu_2O films.[38–40] Further optimization of device performance was thus focused on using the two-step method since the residual PbI_2 provides the beneficial effect of passivation.[41]

Fig. 2b presents the current density–voltage (*J*–*V*) curves of the perovskite solar cells using Cu_2O as the HTM. We observed significant dependence of the solar cell performance on the thickness of the Cu_2O layers. PCE, fill factor (FF) and the short-circuit current density (J_{sc}) decrease with increasing Cu_2O layer thickness (Table 1). This can be attributed to the increases of absorption (Fig. S3†) and series resistance associated with thicker Cu_2O layers. When the Cu_2O layer was 5 nm, a champion device with a PCE of 11.0% was achieved, with a J_{sc} of 17.5 mA cm^{-2}, an open-circuit voltage (V_{oc}) of 0.95 V and a FF of 66.2%. Cu_2O layers thinner than 5 nm resulted in poor coverage and high leakage current. The observed V_{oc} of 0.95 V is much higher than that of the solar cells with CuI HTM (0.55 V),[18] which presumably can be attributed to the lower valence band of Cu_2O in reference to CuI. Comparing with the state-of-the-art inorganic HTMs reported so far (see Table S1†), Cu_2O is clearly a very competitive candidate. The incident photon-to-current efficiency (IPCE) of the device is shown in Fig. 2c, which is featured with a high platform between 350 nm and 700 nm with the maximum of 78% at 620 nm. The integrated current density was calculated to be 17.6 mA cm^{-2}, which is consistent with the measurement results given in Fig. 2b.

Table 1 Dependence of solar cell performance on the Cu_2O layer thickness

Cu_2O thickness (nm)	J_{sc} (mA cm^{-2})	V_{oc} (V)	FF (%)	PCE (%)	R_s (Ohm cm^2)	R_{sh} (Ohm cm^2)
0	8.3	0.576	30.7	1.47	47.9	54.9
5	17.5	0.952	66.2	11.03	7.6	555.6
10	13.3	0.947	57.4	7.20	13.3	568.2
20	9.9	0.941	50.3	4.69	19.1	1250.0
40	7.1	0.940	45.6	3.04	31.4	862.6

Anomalous photocurrent hysteresis was observed during the current–voltage measurements (see Fig. S5†). With voltage scanning in the direction of forward-bias (FB) to short-circuit (SC) conditions, the solar cell showed a higher FF (66.2%) and lower J_{sc} (17.50 mA cm^{-2}) than those of scanning in the SC-to-FB direction (FF: 58.0%; J_{sc}: 18.47 mA cm^{-2}), corresponding to a higher PCE (11.0%) for FB-to-SC than that for SC-to-FB (10.1%). The differences in J_{sc} and FF were likely due to the migration of defects near the perovskite/charge transporter interfaces.[42–44] The charge trapping and polarization effect could also contribute to the slow dynamics of transport measurements.[44] Nevertheless, by applying a bias at the maximum power point (0.74 V), we confirmed that the PCE of 11% could be reliably achieved.

The stability of perovskite solar cells with Cu_2O as the HTM was also characterized and the results are shown in Fig. S6.† Interestingly, J_{sc} reached the peak value only after several days of storage and measurements, which might be caused by the light soaking effect.[45] The PCE of the solar cells without encapsulation kept decreasing during the stability test, which is mainly a result of the decreases of V_{oc} and FF. The underlying reason could be the oxidation and degradation of the perovskite due to the penetration of oxygen and moisture.[46] The histogram plot of PCE for solar cells is shown in Fig. 2d. About half of the devices exhibited PCE above 8%, indicating the consistent high performance of Cu_2O as an HTM. The statistical information of J_{sc}, V_{oc} and FF of these perovskite solar cells is summarized in Fig. S7.†

The performance of perovskite solar cells, especially photocurrent and FF, is closely related to the thickness and morphology of the perovskite layers.[6,7] In comparison with the mesoporous structured solar cells, the planar ones offer more freedom in controlling the device size and film morphology.[8,9] As shown in the SEM image (Fig. 3a), the perovskite grains appear to be uniform, with an average size of approximately 350 nm. Such large grain sizes are favorable for transporting and collecting photo-generated carriers, while suppressing the defect-induced carrier recombination at the grain boundaries.[9]

As shown in Fig. S8,† the energy dispersive X-ray (EDAX) measurements confirmed the presence of all elements in the layers, including Cu. The cross-sectional SEM image of the

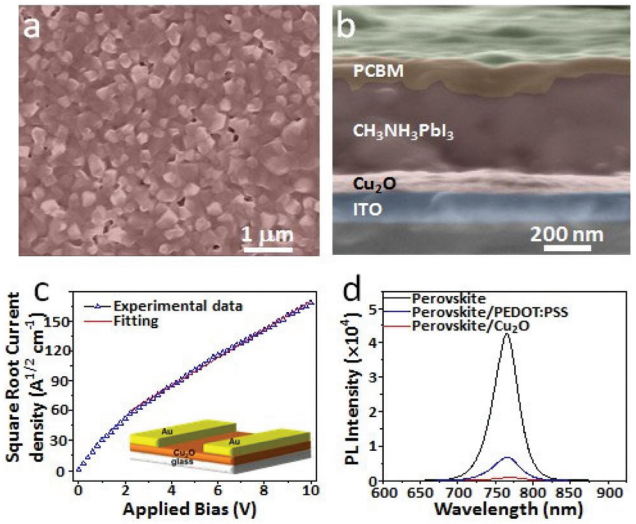

Fig. 3 (a) Top-view SEM image of the $Cu_2O/CH_3NH_3PbI_3$ perovskite layer. (b) Cross-sectional SEM image of the perovskite solar cell. (c) SCLC measurement of the Cu_2O layer. The inset shows the measurement configuration. (d) Steady state photoluminescence of the perovskite layers fabricated on glass, PEDOT:PSS/glass and Cu_2O/glass substrates.

solar cell (Fig. 3b) indicates that all the layers appear to be uniform and the perovskite layer was fully covered by PCBM. The thicknesses of the perovskite and the PCBM layers are approximately 400 nm and 50 nm, respectively. Importantly, PCBM infiltrated between perovskite grains, which facilitates effective charge generation and transportation.

The carrier mobility of HTMs plays a key role in achieving highly efficient solar cells because it helps reduce the series resistance and enhance the FF. As shown in Fig. 3c, the current–voltage curve measured on a Cu_2O layer can be described by the space-charge-limited current (SCLC) model:

$$J = \frac{9}{8}\varepsilon_0\varepsilon\mu\frac{V^2}{d^3} \quad (3)$$

where ε_0 is the permittivity of free space (8.85×10^{-12} F m^{-1}), ε is the dielectric constant of Cu_2O (= 7.5), μ is the charge carrier mobility, and d is the film thickness (40 nm). From the data fitting, we calculated the hole mobility of the Cu_2O layer to be 0.49 cm^2 V^{-1} s^{-1}, which is much higher than those of organic counterparts like spiro-MeOTAD and PEDOT:PSS.[47,48] In comparison, the carrier mobility of spiro-MeOTAD increased from 1.6×10^{-4} cm^2 V^{-1} s^{-1} to 1.6×10^{-3} cm^2 V^{-1} s^{-1} after doping with lithium salts,[47] and the carrier mobility of PEDOT:PSS can reach 1.28×10^{-2} cm^2 V^{-1} s^{-1} after annealing.[48]

To understand the role of the Cu_2O layer in perovskite solar cells and the properties of interfaces, we performed steady-state photoluminescence (PL) measurements. Fig. 3d presents the steady state photoluminescence of a perovskite and a perovskite deposited on various HTMs. Under the same conditions, all samples exhibit a PL peak at 760 nm; however, compared to the pure perovskite film, the PL summit values of the perovskite are largely reduced when interfacing with HTM layers. Such a dramatic PL quenching is particularly interesting in solar cell research because it could be caused by the significantly enhanced charge carrier extraction from the perovskite layer to the electrode. In particular, the PL data show that less than 2% of the PL peak height at 760 nm remained when the Cu_2O layer was introduced as the HTM, which is much better than that of PEDOT:PSS (16% left). Since the Cu_2O thin film has a high carrier mobility and a narrow barrier between the valence band of the perovskite and the work function of Cu_2O (Fig. 3c), a fast carrier transfer from the perovskite to Cu_2O is thermodynamically favored. The observed significant PL quenching unambiguously suggests Cu_2O as an effective HTM for perovskite solar cells.

To further understand the role of the Cu_2O layer in working solar cell devices, we utilized nanosecond transient absorption (ns-TA) spectroscopy to investigate the exciton relaxation dynamics of perovskite/Cu_2O bilayers. For comparison, the same experiment was performed on a sample replacing Cu_2O with PEDOT:PSS/glass. As a reference, a sample of a perovskite layer fabricated on glass without an HTM was also measured. As shown in Fig. 4a, the photobleaching band of the perovskite layer at 760 nm is observed, which is consistent with the steady-state PL quenching experiment. The kinetic decay traces of photobleaching features are presented in Fig. 4b, which are fitted to a double exponential function. The decay components of τ_1 and τ_2 were ascribed to bimolecular recombination and free carrier recombination, respectively (Table S3†).[49–52] Comparison between these three samples gives valuable insights on the role of HTMs in photovoltaic operation. The faster decay component τ_1 of the perovskite film (3.88 ns) on Cu_2O is smaller than those of samples on glass (5.51 ns) and PEDOT:PSS/glass (9.11 ns), suggesting a faster bimolecular recombination and stronger electronic coupling between the perovskite and Cu_2O layer. The slower time constant τ_2 is related to the excited-state decay and carrier recombination dynamics in the perovskite layers.[49,50] The τ_2 value of the perovskite/Cu_2O sample is approximately 50% higher than that of the perovskite on glass, indicating that the photo-excited carriers in the perovskite solar cells with the Cu_2O HTM have a longer lifetime and more opportunities for being collected by the electrodes. When the time delay is above 100 ns, Cu_2O showed a very similar performance to PEDOT:PSS, the well-known HTM for

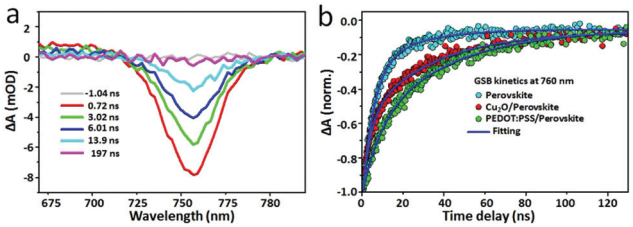

Fig. 4 (a) Transient absorption spectra of perovskites on different substrates at time delays from –1 ns to 197 ns. (b) Kinetics of GSB recovery at 760 nm for perovskite layers on different substrates.

solar cells. To corroborate this observation, we fabricated and measured solar cells using PEDOT:PSS as the HTM. This device showed an efficiency of 12.1% (Fig. S9†), comparable to the Cu_2O device, confirming that Cu_2O is a very competitive HTM for perovskite solar cells.

Conclusions

In summary, we demonstrated the application of ultrathin p-type Cu_2O derived from simple oxidization as a promising inorganic HTM in perovskite solar cells. The scarcity of high-performance p-type inorganic semiconductors makes Cu_2O a valuable addition to the family of charge transporters for perovskite photovoltaic applications. Our experiments revealed that both the thickness and the properties of Cu_2O layers must be carefully tailored in order to achieve the optimal solar cell performance. Using the two-step method to prepare the perovskite layer, a PCE of 11.0% was achieved under AM 1.5 G illumination with ultrathin (5 nm) Cu_2O films as HTMs. The ultrathin nature of the Cu_2O film helps in reducing the material consumption and manufacture cost in the large-scale production of perovskite solar cells. The high performance of such perovskite solar cells can be attributed to the unique properties of the prepared Cu_2O layers, including high hole mobility, well-matched energy levels, and long lifetime of photo-excited carriers. Combining the merits of low cost, facile synthesis, and high device performance, Cu_2O holds promise for facilitating the developments of industrial-scale perovskite solar cells.

Experimental details

Synthesis

Methylammonium iodide (CH_3NH_3I) was prepared according to a previous report.[32] Briefly, 27.86 ml methylamine (40% in methanol) and 30 ml hydroiodic acid (57 wt% in water) were mixed at 0 °C and stirred for 2 h. The precipitate was recovered by evaporation at 50 °C for 1 h. The product was washed with diethyl ether three times and finally dried at 60 °C in a vacuum oven for 24 h. Lead iodide (PbI_2) was purchased from Aldrich and was recrystallized twice before use.

Solar cell fabrication

A thin layer of Cu was first sputtered onto ITO glass (Equipment Support Co., Cambridge, England), then the Cu_2O phase was achieved *via* annealing the ITO/Cu on a hotplate in air at 250 °C for an hour. The film thickness was carefully controlled by the sputtering time. The substrate was then transferred into a glove box immediately for the following process. The perovskite layer was fabricated by a two-step method onto ITO/Cu_2O substrates. PbI_2 solution (0.46 g ml^{-1} in DMF) was spin-coated at 2000 rpm for 45 s. Then the PbI_2 film was annealed at 100 °C on a hotplate for 15 min. After cooling down, the devices were dipped into MAI solution (10 mg ml^{-1} in iso-propanol) for 30 s. After washing with iso-propanol, the devices were heated at 70 °C for 30 min and then at 130 °C for 10 min. A layer of phenyl-C61-butyric acid methyl ester (PCBM, 15 mg ml^{-1} in chlorobenzene) was then spin coated on top of the perovskite film. Finally, an Ag layer (120 nm) was evaporated in a vacuum as top electrodes. For PL or transient absorption measurements, the samples were prepared as mentioned above except that no Ag layer was needed. The perovskite films were finally covered with a poly(methyl methacrylate) (PMMA) layer *via* spin coating a 10 wt% chlorobenzene solution at 2000 rpm for 30 s.

Characterization

UV-Vis spectra were recorded using a JASCO V-670 spectrophotometer equipped with an integrating sphere. X-ray diffraction (XRD) was performed at room temperature using an X-ray diffractometer (D8 Discover, Bruker). Atomic force microscopy (AFM) characterization was conducted on a Bruker's Dimension Icon system. XPS measurements were carried out in a Kratos Axis Ultra DLD spectrometer equipped with a monochromatic Al Kα X-ray source ($h\nu$ = 1486.6 eV) operating at 150 W. The spectra were recorded using an aperture slot of 300 μm × 700 μm. The survey and high-resolution spectra were collected at fixed analyser pass energies of 160 eV and 20 eV, respectively. The samples were mounted in the floating mode in order to avoid differential charging. The current density–voltage (J–V) measurements were conducted on an OAI Trisol tester system combined with a Keithley 2400 source-meter. The light intensity was calibrated to be 100 mW cm^{-2} before measurements. The incident photon-to-current efficiency (IPCE) of the device was measured by using an Oriel IQE200 quantum efficiency measurement system.[53] The morphology of the samples was investigated using an FEI Nova Nano 630 scanning electron microscope (SEM). Photoluminescence measurement was conducted on a Horiba Armis equipment and the excitation light source was a 632 nm laser. For the nanosecond transient absorption spectroscopy, a few μJ of pulse energy as the fundamental output from a Ti:sapphire femtosecond regenerative amplifier (800 nm, 35 fs FWHM, 1 kHz, Newport Spectra-Physics) was used to generate pump and probe beams. By introducing the fundamental beams into an optical parametric amplifier (Light Conversion Ltd), we could select a certain wavelength from the tunable output (240–2600 nm) as the pump pulses, whereas light continuum probe pulses were obtained by focusing the fundamental beams onto a 2 mm-thick sapphire plate (contained in an Ultrafast System LLC spectrometer). The pump and probe pulses overlapped by a small angle of less than 5° on the perovskite samples. The transmitted probe light from the samples was collected and focused on the broadband VIS-NIR detector for recording the time-resolved excitation induced difference spectrum (ΔOD). Details of the TA setup are published elsewhere.[54]

Acknowledgements

This work was supported by King Abdullah University of Science and Technology (KAUST). Dr W. Yu acknowledges the

support from the National Natural Science Foundation of China (NSFC 21404015).

Notes and references

1 S. Kazim, M. K. Nazeeruddin, M. Gratzel and S. Ahmad, *Angew. Chem., Int. Ed.*, 2014, **53**, 2812.
2 M. A. Green, A. Ho-Baillie and H. J. Snaith, *Nat. Photonics*, 2014, **8**, 506.
3 A. Kojima, K. Teshima, Y. Shirai and T. Miyasaka, *J. Am. Chem. Soc.*, 2009, **131**, 6050.
4 J.-H. Im, C.-R. Lee, J.-W. Lee, S.-W. Park and N.-G. Park, *Nanoscale*, 2011, **3**, 4088.
5 H.-S. Kim, C.-R. Lee, J.-H. Im, K.-B. Lee, T. Moehl, A. Marchioro, S.-J. Moon, R. Humphry-Baker, J.-H. Yum, J. E. Moser, M. Graetzel and N.-G. Park, *Sci. Rep.*, 2012, **2**, 591.
6 M. M. Lee, J. Teuscher, T. Miyasaka, T. N. Murakami and H. J. Snaith, *Science*, 2012, **338**, 643.
7 H. Zhou, Q. Chen, G. Li, S. Luo, T.-B. Song, H.-S. Duan, Z. Hong, J. You, Y. Liu and Y. Yang, *Science*, 2014, **345**, 542.
8 D. Liu and T. L. Kelly, *Nat. Photonics*, 2014, **8**, 133.
9 J.-H. Im, I.-H. Jang, N. Pellet, M. Graetzel and N.-G. Park, *Nat. Nanotechnol.*, 2014, **9**, 927.
10 N. J. Jeon, J. H. Noh, W. S. Yang, Y. C. Kim, S. Ryu, J. Seo and S. I. Seok, *Nature*, 2015, **517**, 476.
11 A. Hagfeldt, G. Boschloo, L. Sun, L. Kloo and H. Pettersson, *Chem. Rev.*, 2010, **110**, 6595.
12 X. Chen and S. S. Mao, *Chem. Rev.*, 2007, **107**, 2891.
13 A. Bera, K. Wu, A. Sheikh, E. Alarousu, O. F. Mohammed and T. Wu, *J. Phys. Chem. C*, 2014, **118**, 28494.
14 H. Wang, A. D. Sheikh, Q. Feng, F. Li, Y. Chen, W. Yu, E. Alarousu, C. Ma, M. A. Haque, D. Shi, Z.-S. Wang, O. F. Mohammed, O. M. Bakr and T. Wu, *ACS Photonics*, 2015, **2**, 849.
15 J. H. Heo, S. H. Im, J. H. Noh, T. N. Mandal, C.-S. Lim, J. A. Chang, Y. H. Lee, H.-J. Kim, A. Sarkar, Md. K. Nazeeruddin, M. Graetzel and S. I. Seok, *Nat. Photonics*, 2013, **7**, 486.
16 N. J. Jeon, J. Lee, J. H. Noh, M. K. Nazeeruddin, M. Graetzel and S. I. Seok, *J. Am. Chem. Soc.*, 2013, **135**, 19087.
17 P. Qin, S. Tanaka, S. Ito, N. Tetreault, K. Manabe, H. Nishino, M. K. Nazeeruddin and M. Gratzel, *Nat. Commun.*, 2014, **5**, 3834.
18 J. A. Christians, R. C. M. Fung and P. V. Kamat, *J. Am. Chem. Soc.*, 2014, **136**, 758.
19 W. Yan, Y. Li, Y. Li, S. Ye, Z. Liu, S. Wang, Z. Bian and C. Huang, *Nano Energy*, 2015, **16**, 428.
20 Q. Wang, C. Bi and J. Huang, *Nano Energy*, 2015, **15**, 275.
21 S. Ye, W. Sun, Y. Li, W. Yan, H. Peng, Z. Bian, Z. Liu and C. Huang, *Nano Lett.*, 2015, **15**, 3723.
22 U. Bansode, R. Naphade, O. Game, S. Agarkar and S. Ogale, *J. Phys. Chem. C*, 2015, **119**, 9177.
23 J. Meyer, S. Hamwi, M. Kröger, W. Kowalsky, T. Riedl and A. Kahn, *Adv. Mater.*, 2012, **24**, 5408.
24 Y. Zhao, A. M. Nardes and K. Zhu, *Appl. Phys. Lett.*, 2014, **104**, 213906.
25 P. Gao, M. Gratzel and M. K. Nazeeruddin, *Energy Environ. Sci.*, 2014, **7**, 2448.
26 S. Kazim, M. K. Nazeeruddin, M. Gratzel and S. Ahmad, *Angew. Chem., Int. Ed.*, 2014, **53**, 2812.
27 J. Y. Jeng, K. C. Chen, T. Y. Chiang, P. Y. Lin, T. D. Tsai, Y. C. Chang, T. F. Guo, P. Chen, T. C. Wen and Y. J. Hsu, *Adv. Mater.*, 2014, **26**, 4107.
28 Z. Zhu, Y. Bai, T. Zhang, Z. Liu, X. Long, Z. Wei, Z. Wang, L. Zhang, J. Wang, F. Yan and S. Yang, *Angew. Chem., Int. Ed.*, 2014, **53**, 12571.
29 M. D. Irwin, D. B. Buchholz, A. W. Hains, R. P. H. Chang and T. J. Marks, *Proc. Natl. Acad. Sci. U. S. A.*, 2008, **105**, 2783.
30 K. C. Wang, J. Y. Jeng, P. S. Shen, Y. C. Chang, E. W. G. Diau, C. H. Tsai, T. Y. Chao, H. C. Hsu, P. Y. Lin, P. Chen, T. F. Guo and T. C. Wen, *Sci. Rep.*, 2014, **4**, 4756.
31 A. Paracchino, V. Laporte, K. Sivula, M. Grätzel and E. Thimsen, *Nat. Mater.*, 2011, **10**, 456.
32 Y. Kitagawa, Y. Hiraoka, T. Honda, T. Ishikura, H. Nakamura and T. Kimura, *Nat. Mater.*, 2010, **9**, 797.
33 O. Chmaissem, J. D. Jorgensen, S. Short, A. Knizhnik, Y. Eckstein and H. Shaked, *Nature*, 1999, **397**, 45.
34 Y. Wang, Z. G. Xia, J. Liang, X. W. Wang, Y. M. Liu, C. Liu, S. D. Zhang and H. Zhou, *Semicond. Sci. Technol.*, 2015, **30**, 054004.
35 C. Zuo and L. Ding, *Small*, 2015, **11**, 5528.
36 W.-Y. Yang and S.-W. Rhee, *Appl. Phys. Lett.*, 2007, **91**, 232907.
37 Y. Nakano, S. Saeki and T. Morikawa, *Appl. Phys. Lett.*, 2009, **94**, 022111.
38 J. Li, Z. Mei, L. Liu, H. Liang, A. Azarov, A. Kuznetsov, Y. Liu, A. Ji, Q. Meng and X. Du, *Sci. Rep.*, 2014, **4**, 7240.
39 K. D. Liang, C. H. Huang, C. C. Lai, J. S. Huang, H. W. Tsai, Y. C. Wang, Y. C. Shih, M. T. Chang, S. C. Lo and Y. L. Chueh, *ACS Appl. Mater. Interfaces*, 2014, **6**, 16537.
40 M. M. Tavakoli, L. Gu, Y. Gao, C. Reckmeier, J. He, A. L. Rogach, Y. Yao and Z. Fan, *Sci. Rep.*, 2015, **5**, 14083.
41 D. H. Cao, C. C. Stoumpos, C. D. Malliakas, M. J. Katz, O. K. Farha, J. T. Hupp and M. G. Kanatzidis, *APL Mater.*, 2014, **2**, 091101.
42 E. L. Unger, E. T. Hoke, C. D. Bailie, W. H. Nguyen, A. R. Bowring, T. Heumueller, M. G. Christoforo and M. D. McGehee, *Energy Environ. Sci.*, 2014, **7**, 3690.
43 X. Zheng, B. Chen, C. Wu and S. Priya, *Nano Energy*, 2015, **17**, 269.
44 R. S. Sanchez, V. Gonzalez-Pedro, J.-W. Lee, N.-G. Park, Y. S. Kang, I. Mora-Sero and J. Bisquert, *J. Phys. Chem. Lett.*, 2014, **5**, 2357.
45 C. E. Small, S. Chen, J. Subbiah, C. M. Amb, S.-W. Tsang, T.-H. Lai, J. R. Reynolds and F. So, *Nat. Photonics*, 2012, **6**, 115.

46 A. D. Sheikh, A. Bera, M. A. Haque, R. B. Rakhi, S. D. Gobbo, H. N. Alshareef and T. Wu, *Sol. Energy Mater. Sol. Cells*, 2015, **137**, 6.
47 H. J. Snaith and M. Grätzel, *Appl. Phys. Lett.*, 2006, **89**, 262114.
48 S. A. Rutledge and A. S. Helmy, *J. Appl. Phys.*, 2013, **114**, 133708.
49 Q. Chen, H. Zhou, T.-B. Song, S. Luo, Z. Hong, H.-S. Duan, L. Dou, Y. Liu and Y. Yang, *Nano Lett.*, 2014, **14**, 4158.
50 L. Zuo, Z. Gu, T. Ye, W. Fu, G. Wu, H. Li and H. Chen, *J. Am. Chem. Soc.*, 2015, **137**, 2674.
51 S. D. Stranks, G. E. Eperon, G. Grancini, C. Menelaou, M. J. P. Alcocer, T. Leijtens, L. M. Herz, A. Petrozza and H. J. Snaith, *Science*, 2013, **342**, 341.
52 G. Xing, N. Mathews, S. Sun, S. S. Lim, Y. M. Lam, M. Graetzel, S. Mhaisalkar and T. C. Sum, *Science*, 2013, **342**, 344.
53 M. I. Saidaminov, A. L. Abdelhady, B. Murali, E. Alarousu, V. M. Burlakov, W. Peng, I. Dursun, L. Wang, Y. He, G. Maculan, A. Goriely, T. Wu, O. F. Mohammed and O. M. Bakr, *Nat. Commun.*, 2015, **6**, 7586.
54 O. F. Mohammed, D. Xiao, V. S. Batista and E. T. J. Nibbering, *J. Phys. Chem. A*, 2014, **118**, 3090.